Surface & Coatings Technology 205 (2010) 1624–1629

Contents lists available at ScienceDirect

Surface & Coatings Technology

journal homepage: www.elsevier.com/locate/surfcoat

Osteoblast growth behavior on micro-arc oxidized β-titanium alloy

Hsien-Te Chen [a,b], Chi-Jen Chung [c,*], Tsai-Ching Yang [a], I-Ping Chiang [d], Chin-Hsin Tang [e], Keh-Chang Chen [a], Ju-Liang He [a]

[a] Department of Materials Science and Engineering, Feng Chia University, 100 Wen-Hwa Road, Taichung 40724, Taiwan, ROC
[b] Department of Orthopaedic Surgery, China Medical University Hospital, School of Chinese Medicine, China Medical University, 2 Yue-Der Road, Taichung 40447, Taiwan, ROC
[c] Department of Dental Technology and Materials Science, Central Taiwan University of Science and Technology, 666 Buzih Road, Beitun District, Taichung 40601, Taiwan, ROC
[d] Department of Pathology, China Medical University Hospital, 2 Yue-Der Road, Taichung 40447, Taiwan, ROC
[e] Department of Pharmacology, China Medical University, 91 Hsueh-Shih Road, Taichung 40421, Taiwan, ROC

ARTICLE INFO

Available online 16 July 2010

Keywords:
β-titanium
Micro-arc oxidation (MAO)
Titanium dioxide (TiO_2)
Osteogenesis
In vivo
In vitro

ABSTRACT

β-titanium (β-Ti) alloys are known for their excellent physical properties and biocompatibility, and are therefore considered as next-generation metals for orthopedics and dental implants. To improve the osseous integration between β-Ti alloys and bone, this study develops a titanium dioxide (TiO_2) coating on the surface of β-Ti alloys by using micro-arc oxidation (MAO) technique. The anatase (A) rich and rutile (R) rich TiO_2 layer, were formed on β-Ti, respectively. *In vitro* tests were carried out using pre-osteoblast cell (MC3T3-E1) to determine biocompatibility and bone formation performance. Biocompatibility includes cell adhesion, cell proliferation, and alkaline phosphatase (ALP) activity, while the bone formation performance contains osteopontin (OPN), osteocalcin (OCN) and calcium content. Cell morphology was also observed. In addition, raw β-Ti, A rich TiO_2 and R rich TiO_2 were implanted into the distal femora of Japanese white rabbits for 4, 8, and 12 weeks to evaluate its *in vivo* performance.

Experimental results show that TiO_2 coating can be grown on and well-adhered to β-Ti. The anatase phase formed under a low applied voltage (350 V), while the rutile phase formed under a high applied voltage (450 V), indicating that crystal structure is strongly influenced by applied voltage. A porous morphology was obtained in the TiO_2 coating regardless of the crystal structure and exhibited superior bone formation performance than β-Ti. *In vivo* analysis and *in vitro* test show similar trends. It is also noticeable that the R rich TiO_2 coating achieved better biocompatibility, osteogenesis performance. Therefore, a MAO-treated R rich TiO_2 coating can serve as a novel surface modification technique for β-Ti alloy implants.

1. Introduction

The choice of scaffold materials plays an important role in tissue engineering [1]. Commonly-used scaffold materials for various diseases or trauma situation include collagen, gelatin, biodegradable polyglycolide (PLA), polylactides (PGA) [1–5], 316 L stainless steel, Co–Cr–Mo alloy and titanium alloys, etc. Of these materials, β-titanium alloys (β-Ti) benefit from their excellent physical properties and biocompatibility, and are well known as one of the major materials in orthopedics and dental implants. In addition, the surface characteristics [6,7] of these materials are an important factor in determining *in vitro* cell behavior and bone formation performance.

Micro-arc oxidation (MAO), which produces a TiO_2 coating with the characteristics of high electrolyte variation [8], alternative crystal phase, and a porous structure, can provide strong adhesion force between TiO_2 coating and substrate [8–10]. Our previous study shows that excellent *in vitro* biocompatibility can be achieved by applying an MAO–TiO_2 layer [11] and the osteoblast cell compatibility presented by the treated specimens is increased but less sensitive to the process parameters, even though the associated difference in morphology and crystalline form of the MAO–TiO_2 layers are found to be tremendous. A review of the literature shows that most studies focus on *in vitro* cell biocompatibility [12,13] instead of *in vivo* animal tests. In addition, very little has been addressed on how the types of crystal structure of the MAO–TiO_2 layer really affect bone cell growth in the *in vivo* and *in vitro* conditions. Therefore, this study discusses *in vivo* animal tests in addition to *in vitro* tests to evaluate the feasibility of bone cell growth on the MAO–TiO_2 layers. To determine the compatibility of the living bone cells with implant materials, this study uses MAO to fabricate anatase rich (A rich) and rutile rich (R rich) phase TiO_2 layers on a β-Ti thin plate in both *in vitro* and *in vivo* tests. The pre-osteoblast cell (MC3T3-E1 cell) was cultured *in vitro* on MAO–TiO_2 coatings to observe the cell morphology, biocompatibility, and osteogenesis performance indexes including cell adhesion, cell proliferation, ALP activity, osteopontin (OPN), osteoclacin (OCN) and calcium content. On the other hand, the histological reaction between different

* Corresponding author. Tel./fax: +886 4 24519053.
E-mail address: cjchung@seed.net.tw (C.-J. Chung).

0257-8972/$ – see front matter © 2010 Elsevier B.V. All rights reserved.
doi:10.1016/j.surfcoat.2010.07.027

materials (raw β-Ti, A rich and R rich TiO_2 implants) and bone are investigated in the *in vivo* animal test.

2. Experimental

2.1. Specimen preparation

A new β-Ti alloy, Ti–13Cr–3Al–1Fe (Trade name: CA–Ti), was purchased from Japan Daido Steel and used as a substrate. The substrates were cut into dimension of 20.0 mm × 20.0 mm × 1.0 mm for microstructure characterization of TiO_2 coatings and dimension of 10.0 mm × 10.0 mm × 1.0 mm for *in vitro* and *in vivo* tests. Table 1 shows the MAO treatment parameters used in this study, where the crystal structure and microstructure of the TiO_2 layer can be well-controlled by adjusting the applied voltage. A Bruker-D8 X-ray diffractometer (XRD), using Cu Kα (λ = 1.5405 nm) radiation was employed to identify the crystal structure of the MAO-treated TiO_2 layer. The cross-sectional morphology and film thickness were established using a Hitachi S-4800 cold field emission scanning electron microscope (FESEM), whereas the surface elemental composition of β-Ti alloy before and after MAO treatment were identified by energy dispersive spectrometer (EDS). In addition to the A rich and R rich TiO_2 specimens, the raw α-Ti and β-Ti alloy were used as control groups in the following biocompatibility tests.

2.2. In vitro osteoblast biocompatibility and osteogenesis performance assay

In vitro tests included the evaluation of cell adhesion, cell proliferation, ALP activity, osteogenesis performance, and cell morphology. A murine pre-osteoblast cell line MC3T3-E1 was obtained from Riken Cell Bank (Tsukuba, Japan). In the cell adhesion assay, the labeled pre-osteoblasts cells were plated in test specimens and incubated for 2 h at 37 °C to allow adhesion. After being washed twice with phosphate buffered saline (PBS), the non-adherent cells were removed by aspiration and the plates were read with CytoFluor 2300 fluorescence plate reader (Millipore) to determine the fluorescence intensity as an indication of cell adhesion. To determine cell proliferation, the cell viability was measured using MTT (3-[4,5-dimethylthiahiazo-2-yl]-2,5-diphenytetrazolium bromide) assay protocol. The MC3T3-E1 cells were cultured for 48 h on various coated specimens at a density of 10^4 cells/cm^2. Finally, absorbance at 550 nm was used as an indication for cell proliferation determined using a microplate reader (Bio-Tek, Winooski, VT). ALP activity was measured using an ALP assay kit (Sigma, CA). MC3T3-E1 cells were cultured onto test specimens (10^4 cells/cm^2) for 2 days. Finally, the absorbance levels of the supernatant aliquots subjected to protein assay using the Pierce Coomassie Plus assay reagent (Pierce, Rockford, USA) were read at 405 nm (Bio-Tek, Winooski, VT) to determine the ALP activity as an indication for cell differentiation.

Osteogenesis performance was determined by measuring OPN, OCN and calcium content. MC3T3-E1 cells were cultured in test specimens and incubated for 48 h at 37 °C. The OPN and OCN content were assayed using OPN and OCN enzyme immunoassay kits, following the procedure described by the manufacturer (Biocompare; San Jose, CA, USA). The calcium content was evaluated by measuring mineralized nodule formation. The pre-osteoblasts were cultured in α-MEM containing 50 μg/ml vitamin C and 10 mM β-glycerophosphate. Bone nodule formation was determined on the 10th day using alizarin red-S staining and finally the alizarin red-S content in samples was quantified by measuring absorbance at 550 nm and calculated according to a standard curve.

The cells on the test specimens were washed twice, serial dehydrated and critical point dried followed by sputtered-Au coating for cell morphological observation by using a Hitachi S-3000N scanning electron microscope operating in a secondary electron (SE) mode.

Table 1
Micro-arc oxidation treatment parameters used in this study.

Parameters	Data
Chemical composition	Ti–13Cr–3Al–1Fe
Electrolyte	NaH_2PO_4 (0.05 M)
Bath pH	9.2
Applied voltage (V)	350, 450
Oxidizing time (min)	20
Substrate (as anode)	CA–Ti (2 × 2 cm^2, 1 × 1 cm^2)
Cathode material	Stainless steel (4 × 9 cm^2)
Bath stirring	Magnetic stirrer
Bath temp. (°C)	25 °C

2.3. In vivo bone growth test by rabbit transcortical model

All animal experiments were approved by the China Medical University's Institutional Animal Care and Use Committee. A total of fifteen Japanese White male rabbits (weighted 3.6 kg in average) were randomly divided into three groups for embedding three different implants (β-Ti, MAO-treated A rich and R rich TiO_2 on β-Ti) into distal femora. Thus, three possible *in vitro* osteoblast-favored materials; raw β-Ti, A rich, and R rich MAO-treated β-Ti were to determine their *in vivo* behavior. Each implant was embedded into the distal femur of each rabbit along a 10.0 × 1.0 mm drilled-slot, following the canine transcortical model used by Bobyn et al. [14], after the rabbits were anaesthetized. Fig. 1 shows the implantation procedure, where Fig. 1(a) and (b) point out the drilled-slot on a distal femur and implant insertion, respectively.

At 4, 8 and 12 weeks after implantation, each rabbit was euthanized and its femur with implant were excised from the

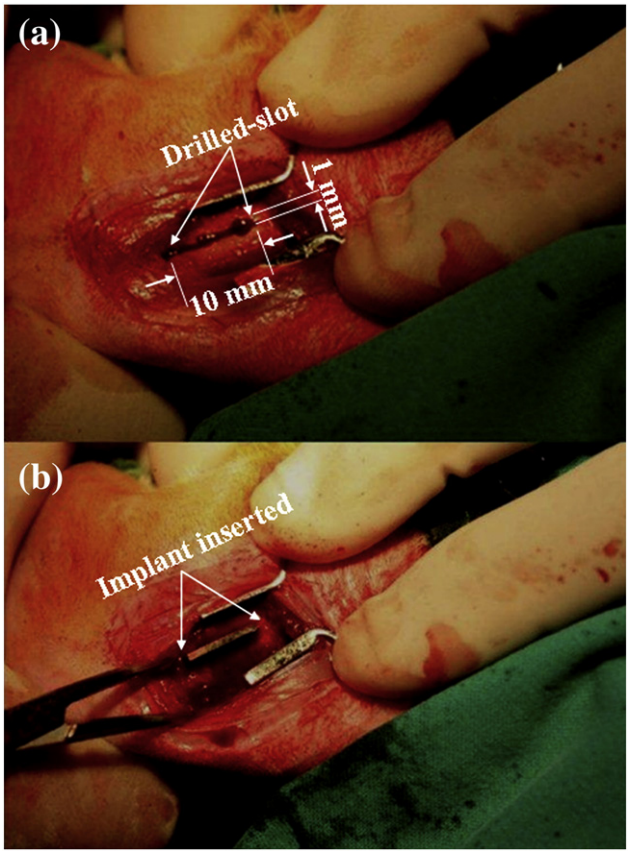

Fig. 1. Implant embedded in distal femora of rabbit (a) created a 10.0 × 1.0 mm drilled-slot, (b) implant embedded in distal femora.

surrounding soft tissue. The excised femora samples were placed into formaldehyde (4%) after being photographed and measured followed by cold-mounted in EpoFix and coagulated at room temperature. Implant-containing bone sections 1 mm thick were obtained using an Accutom-50 machine (Struers A/S, Denmark). They were then progressively ground and polished to 100 μm thick. Each section was stained with hematoxylin and eosin stain (HE stain) and then investigated histomorphology using an optical microscope.

3. Results and discussion

3.1. Crystal structure and microstructure of MAO-treated TiO_2 layer

Fig. 2 shows the XRD pattern and SEM cross-sectional image of MAO-treated (a) A rich and (b) R rich TiO_2 layer structures under different applied voltage. As can be seen, the MAO treatment parameters control the TiO_2 crystal structure to grow A rich phase at low applied voltage (350 V), while R rich phase at high applied voltage (450 V). This is due to the activation energy difference between anatase and rutile. A higher applied voltage facilitated a favorable condition for rutile growth, and vice versa. It had been described in our early paper [11]. At low applied voltage (350 V), the TiO2 layer exhibited abundant pores with small diameter (shown in the surface morphology). Both the pore size and coating thickness (shown in the cross-sectional morphology) increased as the applied voltage was increased. Therefore, the desired phase structure and microstructure of the TiO_2 layer could be achieved by appropriately adjusting MAO parameters.

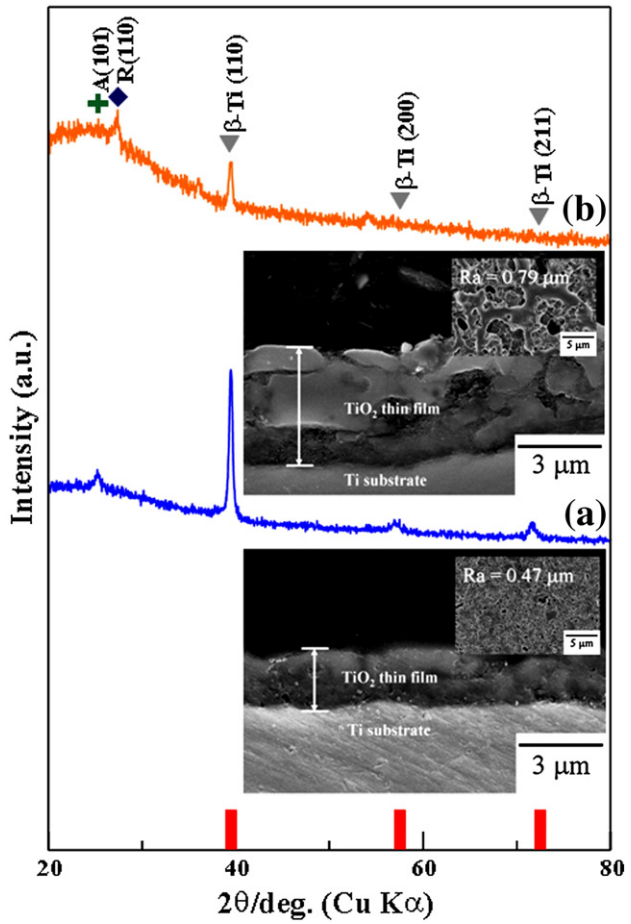

Fig. 2. XRD pattern, cross-sectional and surface morphology of MAO-treated (a) A rich TiO_2 and (b) R rich TiO_2 specimens. XRD peaks of raw β-Ti are marked with red bars in the bottom of this figure.

A similar tendency in coating morphology variations appeared in MAO-treated α-Ti alloy [15,16] and α + β Ti alloy systems [17,18]. After comparing with our previous study and literatures, it is believed that the MAO-treated β-Ti alloy followed the same dielectric breakdown behavior to produce the oxidized TiO_2 layer [11,19,20]. Thus, the obtained crystal structure of MAO-treated β-Ti is predictable and also is able to fabricate on any kinds of titanium alloys due to their similar oxide formation mechanism among different titanium alloys.

Fig. 3 shows the elemental composition of raw β-Ti and the MAO-treated β-Ti alloy. The number of Cr, Al and Fe elements dropped significantly after micro-arc oxidation. This implies that the crystal structure of TiO_2 restricted solubility of these elements into the oxidized layer. The phosphorous content in the MAO-treated specimen, on the contrary, substantially increased gives an implication of a greater bone formation capability and renders the materials more bioactive as well [21]. Moreover, oxygen significantly increased due to the intensive oxidation by the micro-arc.

3.2. In vitro biocompatibility, osteogenesis performance, and cell morphology of osteoblasts on TiO_2 layer

After 2 h cell growth on the specimens, the pre-osteoblasts were conformably attached to all the specimens and the pseudopodia spread out uniformly, as shown in Fig. 4(a), where at the same time, the cells adhered to the A rich and R rich TiO_2 specimens were not much different. However, the cells seemed to adhere more tenaciously and conform to a larger extent on the A rich and R rich TiO_2 specimens in contrast to the raw β-Ti. In addition, the adhered cell number on both A rich and R rich TiO_2 specimens was visually seen in Fig. 4(a) to be greater than that on raw β-Ti. However again, that the proliferation of the cells grown on both A rich and R rich TiO_2 specimens are much better than that on the raw β-Ti in terms of the cell number (proliferation) as well as the manner of cell accommodation. Moreover, the cells accommodate most conformably onto the R rich TiO_2 specimen. This can be ascribed to the fact that the MAO-treated TiO_2 layer accelerates the cell adhesion in the very beginning of cell culture and induced cell proliferation, especially on R rich TiO_2. The *in vitro* bioactivity has been proposed to be associated with the Ti–OH group or negatively charged surface of the anatase structure in our previous study [11]. However, the R rich TiO_2 specimen

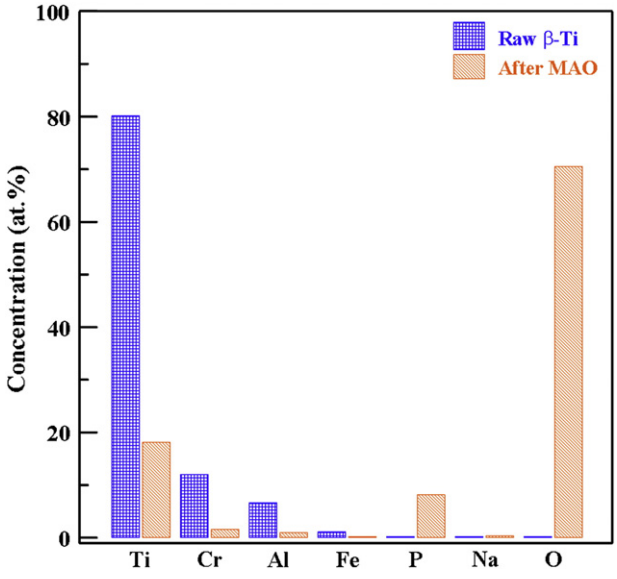

Fig. 3. Surface elemental composition of the raw β-Ti and MAO-treated β-Ti.

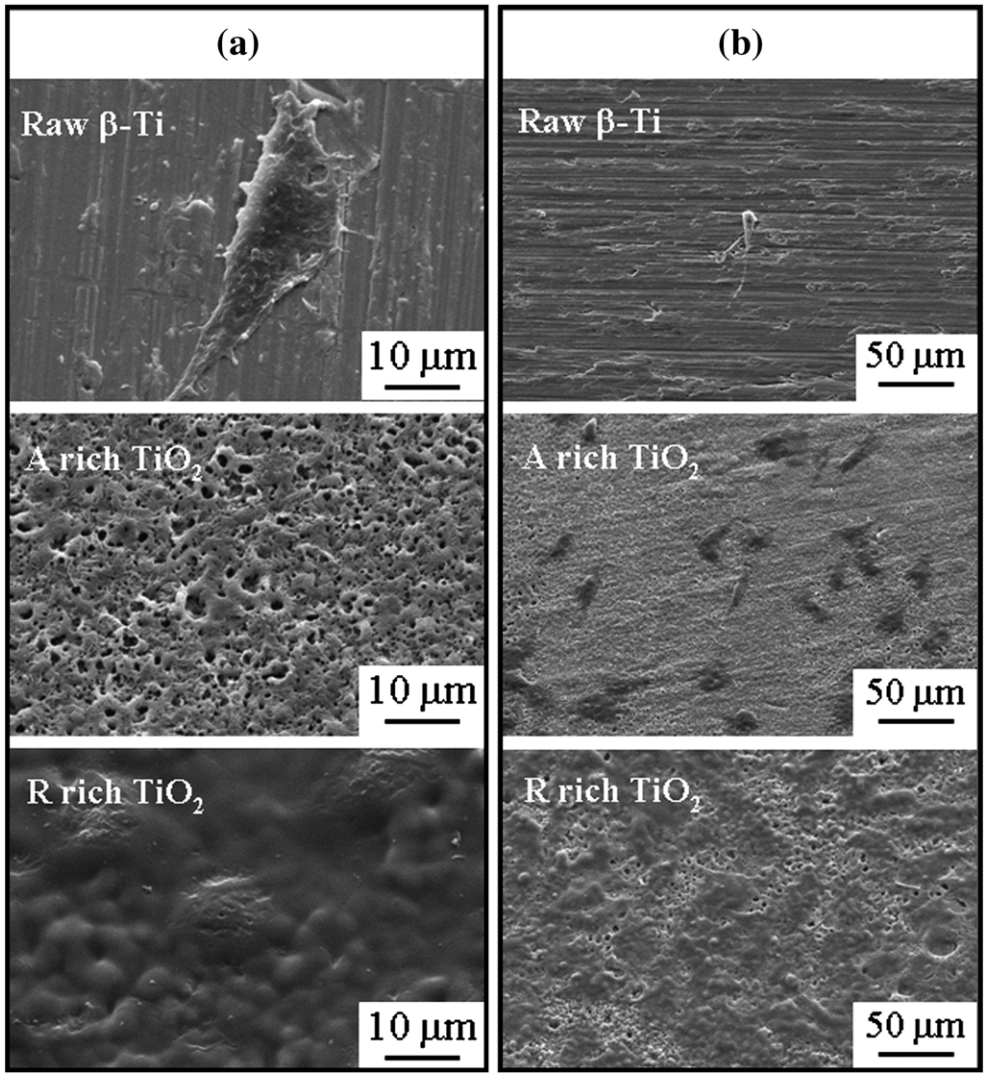

Fig. 4. SEM morphology of MC3T3-E1 cells adhered to (a) raw β-Ti, A rich and R rich TiO_2 specimens for 2 h, and proliferated on (b) raw β-Ti, A rich and R rich TiO_2 specimens for 48 h.

demonstrating even better cell adhesion and proliferation than A rich TiO_2 in this study is similar to the result of Sul et al. who revealed that the Mg-containing R rich TiO_2 exhibited significantly better integration in bone compared to A rich TiO_2 [22]. These results are consistent with *in vitro* experiments, which concluded that cells adhere more strongly and proliferate more on MAO-treated implants than untreated titanium implants [23].

Fig. 5 reveals the quantitative *in vitro* test results of (a) cell adhesion, (b) cell proliferation, (c) ALP activity, (d) OPN, (e) OCN, and (f) calcium content for culturing MC3T3-E1 cells on α-Ti, β-Ti, A rich, and R rich TiO_2 specimens, respectively. In Fig. 5(a), it shows that the raw β-Ti alloy exhibited better cell adhesion performance than β-Ti. This could be ascribed to the chemical nature difference of the naturally grown surface oxide on both metals that contribute different degree of chemical interaction to assist cell adhesion. Meanwhile, both MAO-treated β-Ti showed a substantial increase in cell adhesion (Fig. 5(a)), cell proliferation (Fig. 5(b)) and ALP activity (Fig. 5(c)) than raw titanium specimens. In addition, the R rich TiO_2 specimens demonstrated much higher cell adhesion, cell proliferation, and ALP activity than the other three specimens (α-Ti, β-Ti and A rich TiO_2 layer). This indicates that better osteoblast compatibility occurred in the early cell growth stages to the MAO-treated TiO_2 layer favoring later osteogenesis performance. Therefore, the OPN and OCN values, the important osteoblast markers at bone late-stage differentiation,

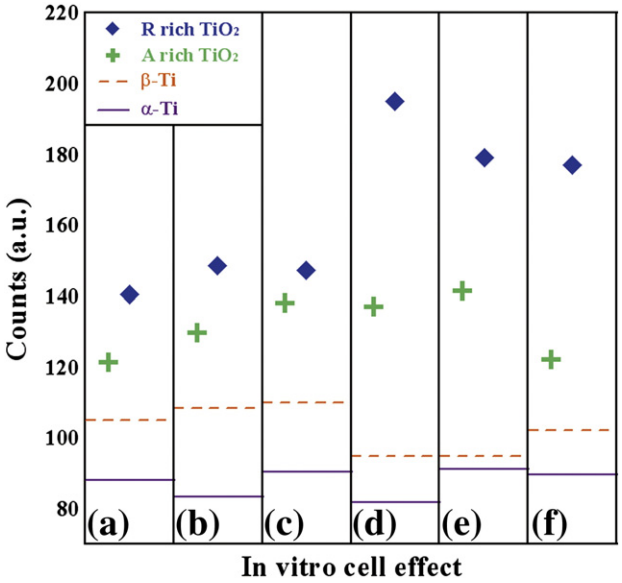

Fig. 5. *In vitro* test result of MC3T3-E1 for (a) cell adhesion, (b) cell proliferation, (c) ALP activity, (d) OPN, (e) OCN, and (f) calcium content on α-Ti, β-Ti, A rich and R rich TiO_2 specimens.

and calcium content were examined. In Fig. 5(d), (e), and (f), the OPN, OCN levels and calcium content showed a significant increase when the osteoblast was cultured on MAO-treated β-Ti alloy. This confirmed the positive effect of MAO-treated β-Ti alloy on osteoblast differentiation. In other words, MC3T3-E1 cells differentiated more quickly on the MAO-treated β-Ti alloy than on the raw β-Ti alloy. These results indicate that osteogenesis is prone to happen on both MAO-treated A rich and R rich TiO_2 structures [15,24,25]. Again, in comparison of A rich and R rich TiO_2, which both possessed similar surface morphology, these two phases, however, showed their differences in all *in vitro* cell tests where R rich TiO_2 exhibited superior behaviors than A rich TiO_2. It is speculated that the R rich TiO_2, exhibits much higher chemical stability on the surface as opposed to the A rich TiO_2 where the surface may undergoes free radical or superion formation constantly. Additional study shall be carried out to reveal the difference in cell response to these two phases. In conclusion, MAO-treated TiO_2 layer, especially the R rich TiO_2, showed the best biocompatibility and osteogenesis performance among all materials evaluated in these *in vitro* tests.

3.3. Effect of MAO-treated β-Ti on in vivo bone growth

For all the experimental rabbits, clinical observations of the surgical wound showed primary wound healing without signs of infection at 4, 8 and 12 weeks. No implant was dislodged or appeared to be loose at the time of retrieval. The experimental rabbits tolerated the implants well. Fig. 6 shows macroscopic images of rabbit femora embedded with different implants (raw β-Ti implants and MAO-treated implants) retrieved at 4, 8, and 12 weeks. Fig. 6(a) reveals different proportional woven bone and soft tissue contacted with the raw β-Ti implants at 4, 8, 12 weeks, and all the implants remained stable. In Fig. 6(b) and (c), mostly irregular bone with a small amount of soft tissue appositional to the MAO-treated β-Ti implants was found in the femora obtained at 4 weeks. Meanwhile, the femora obtained at 8 and 12 weeks shown in Fig. 6(b) and (c) revealed that MAO-treated β-Ti implants closely integrated surrounding compact bone, and the implants were difficult to be removed. An overall comparison of Fig. 6(a), (b) and (c) shows that bone ongrowth occurred more prominently in MAO-treated β-Ti implants, with observable difference between MAO-treated β-Ti implants and raw β-Ti implants.

Histological characteristics were quite obviously different for MAO-treated β-Ti implants and raw β-Ti implant after 8 weeks embedded in rabbit femora in Fig. 7(a), (b), and (c). In each time period during implantation, MAO-treated β-Ti implants showed better bone growth than raw β-Ti implants in terms of ongrowth bone quantity and maturity. At 8 weeks, a small amount of appositional trabeculae new bone appeared at the area close to the interface of implant (Fig. 7(a)). This indicates that the osteogenesis was active, but little bone was formed, and was still immature. Fig. 7 (b) and (c) shows that the area between the bone-implant interface and distal femora is composed of laminated compact bone. Some trabeculae bones have been converted into irregular compact bone. Additionally, some new bones extend from the interface and forms irregular ingrowth, are likely due to growth into the pores on the implant surface. Other than overall design, the implant characteristics that influence the effectiveness of dental implants include surface composition, surface activity, and surface roughness [16]. The MAO-treated TiO_2 layer on β-Ti has a rough, porous surface and forms embedded physical connection with bone tissue after implantation, which facilitates new bone growth into the pores. The results of this study are consistent with *in vivo* experiments, which concluded that surface modification by MAO technique promotes more rapid formation of new bone and increases the bone-implant shear strength compared to untreated titanium implants [26]. It is indistinguishable for *in vivo* bone growth behavior on MAO-treated A rich TiO_2 and R TiO_2 layer, although the R rich TiO_2, showed the best biocompatibility and osteogenesis performance among all *in vitro* tests and materials. Probably, the anatase and rutile crystal structure, respectively in each corresponding MAO-treated specimen are not high enough in content to make a significant difference on *in vivo* bone growth. Thus, future *in vivo* study would be focused on purifying the crystal structure of MAO-treated β-Ti alloy in order to evaluate the difference of *in vivo* bone growth behavior between A rich TiO_2 and R TiO_2 layer on β-Ti alloy

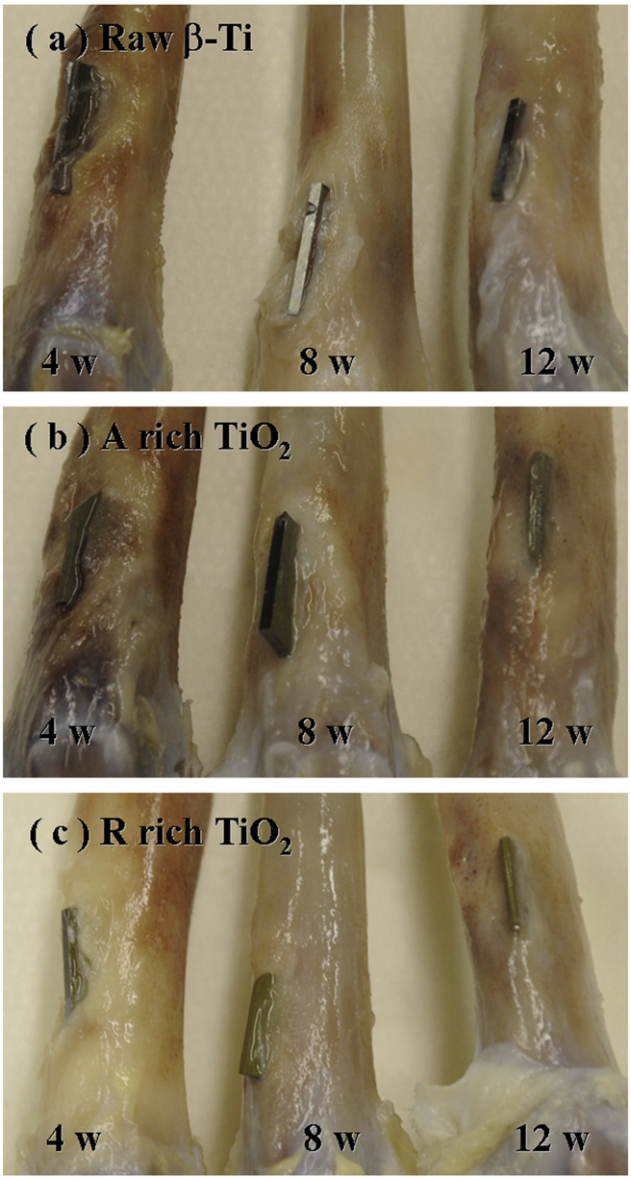

Fig. 6. Macroscopic observation of implant-containing rabbit femora retrieved on the 4th, 8th and 12th weeks after implantation.

4. Conclusions

MAO-treated porous anatase and rutile rich TiO_2 coating can be successfully fabricated on the β-Ti alloy surface and concluded as following:

(a) The crystal structure is prone to form an A rich TiO_2 coating at a relatively low applied voltage of 350 V; and an R rich TiO_2 coating formed at a relatively high applied voltage of 450 V. Both phase structures formed a rough porous layer with firm growth into the substrate.

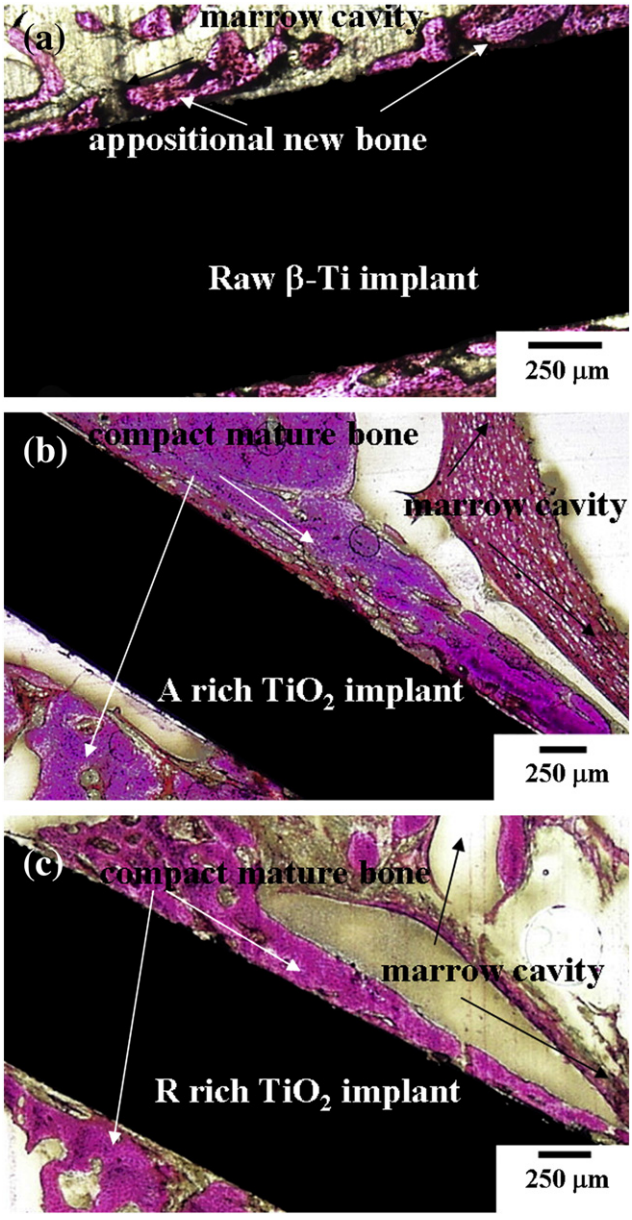

Fig. 7. Histological observations of implant-containing sections at 8 weeks after embedded in rabbit femora (hematoxylin and eosin stain, original magnification 40×).

(b) *In vitro* tests showed that the TiO_2 layer improves osteoblast biocompatibility and calcium deposition performance. Furthermore, R rich TiO_2 layer generally gives better biocompatibility and osteogenesis performance than A rich layer.

(c) The *in vivo* rabbit transcortical model shows that the MAO-treated β-Ti implant can achieve better bone formation and ongrowth in each time period than the raw β-Ti implant. Therefore, the MAO-treated TiO_2 coating may serve as a novel surface modification technique for β-Ti alloy implants for orthopedics and dental implant application.

Acknowledgments

The authors would like to thank Feng Chia University (FCU) and Taichung Veterans General Hospital (TVGH) for funding this work under the Feng-Rong Project (FCU-TCVGH-08G27412). The authors are also grateful to the National Science Council of Taiwan for its financial support under contract NSC 98-2218-E-166-001. Mr. Jimmy Hsu in Kintech Co. for helping histological sample preparation is also deeply appreciated.

References

[1] D.W. Hutmacher, Biomaterials 21 (2000) 2529.
[2] L.G. Griffith, Acta Mater. 48 (2000) 263.
[3] S.L. Ishaug, G.M. Crane, M.J. Miller, A.W. Yasko, M.J. Yaszemsl, A.G. Mikos, J. Biomed. Mater. Res. A 36 (1997) 17.
[4] S.V. Madihally, H.W.T. Matthew, Biomaterials 20 (1999) 1133.
[5] H. Lo, S. Kadiyala, S.E. Guggino, K.W. Leong, J. Biomed. Mater. Res. A 30 (1996) 475.
[6] H.C. Cheng, S.Y. Lee, C.C. Chen, Y.C. Shyng, K.L. Ou, Appl. Phys. Lett. 89 (2006) 173902-1.
[7] K.L. Ou, C.T. Lin, S.L. Chen, C.F. Huang, H.C. Cheng, Y.M. Yeh, K.H. Lin, J. Electrochem. Soc. 155 (2008) E79.
[8] L.H. Li, Y.M. Kong, H.W. Kim, Y.W. Kim, H.E. Kim, S.J. Heo, J.Y. Koak, Biomaterials 25 (2004) 2867.
[9] C.Y. Zheng, S.J. Li, X.J. Tao, Y.L. Hao, R. Yang, L. Zhang, Mater. Sci. Eng. C 27 (2007) 824.
[10] I. Montero, J.M. Albella, J.M. Martinez-Duart, J. Electrochem. Soc. 132 (1985) 976.
[11] H.T. Chen, C.H. Hsiao, H.Y. Long, C.J. Chung, C.H. Tang, K.C. Chen, J.L. He, Surf. Coat. Technol. 204 (2009) 1126.
[12] X.J. Tao, S.J. Li, C.Y. Zheng, J. Fu, Z. Guo, Y.L. Hao, R. Yang, Z.X. Guo, Mater. Sci. Eng. C 29 (2009) 1923.
[13] C.I. Vamanu, M.R. Cimpan, P.J. Høl, S. Sørnes, S.A. Lie, N.R. Gjerdet, Toxicol. Vitro 22 (2008) 1689.
[14] J.D. Bobyn, G.J. Stackpool, S.A. Hacking, M. Tanzer, J.J. Krygier, J. Bone Joint Surg. Br. 81 (1999) 907.
[15] L.H. Li, Y.M. Kong, H.W. Kim, Y.W. Kim, H.E. Kim, S.J. Heo, J.Y. Koak, Biomaterials 25 (2004) 2867.
[16] Y. Han, S.H. Hong, K. Xu, Surf. Coat. Technol. 168 (2003) 249.
[17] Y. Han, S.H. Hong, K.W. Xu, Surf. Coat. Technol. 154 (2002) 314.
[18] Z. Yao, Y. Jiang, Z. Jiang, F. Wang, Z. Wu, J. Mater. Process. Technol. 205 (2008) 303.
[19] H. Ishizawa, M. Ogino, J. Biomed. Mater. Res. A 29 (1995) 65.
[20] Y.T. Sul, C.B. Johansson, S. Petronis, A. Krozer, Y. Jeong, A. Wennerberg, T. Albrektsson, Biomaterials 23 (2002) 491.
[21] J.F. Shackelford, Mater. Sci. Forum 293 (1999) 1.
[22] Y.T. Sul, C. Johansson, E. Byon, T. Albrektsson, Biomaterials 26 (2005) 6720.
[23] W. Ma, B. Liu, X. Wang, Chin. J. Clin Rehabil 8 (2004) 2618.
[24] J.M. Wu, F. Xiao, S. Hayakawa, K. Tsuru, S. Takemoto, A. Osaka, J. Mater. Sci. Mater. Med. 14 (2003) 1027.
[25] M. Sevtina, L.C. Ciacchi, O. Meriani, A. De Vita, Acta Mater. 49 (2001) 2169.
[26] W. Ran, Z.H. Tian, B. Guo, D.L. Shu, K.H. Nan, Y.J. Wang, Biomed. Mater. 4 (2009) 055003-1.